Turk J Pharm Sci 2025;22(3):178-190
DOI: 10.4274/tjps.galenos.2025.56949

ORIGINAL ARTICLE

Physicochemical Characterization, Drug Release, Stability, and Cytotoxicity of Cross-Linked Curdlan-Based Nanosponges for α-Amyrin and Higenamine Delivery

Shailaja Amol DOMBE[1]*, Pramodkumar Jaykumar SHIROTE[2]

[1]Arvind Gavali College of Pharmacy, Department of Pharmaceutics, Satara, India
[2]Shivaji University, Sarojini College of Pharmacy, Department of Pharmaceutical Chemistry, Kolhapur, India

ABSTRACT

Objectives: Michigan cancer foundation-7 (MCF-7) breast-cancer cells are recognized for their resilience against conventional chemotherapy drugs and apoptosis-triggering agents. Nanosponges (NSs) have emerged as promising drug-delivery systems in cancer therapy because of their ability to encapsulate and deliver therapeutic agents efficiently. The aim of this study was to establish the combined beneficial anticancer impacts of NSs alpha-amyrin (AMY) and higenamine (HGN) on MCF-7 breast-cancer cells.

Materials and Methods: NSs were developed using a solvent-evaporation technique that used dichloromethane as the solvent and curdlan as the polymer. A comprehensive randomized 3^2 factorial design was employed to vary curdlan content (X_1) and stirring rate (revolutions per minute, X_2) and to investigate their influence on particle size (Y_1) and entrapment efficiency (EE, Y_2). The optimized formulation then underwent in-vitro investigations, encompassing apoptosis and cell-cycle studies with the MCF-7 breast-cancer cell line.

Results: The prepared NSs (F1-F9) exhibited optimal physical and chemical characteristics. Optimization produced formulation F10, which achieved a particle size of 280.9 nm and an EE of 63.00%. The model was established for all dependent variables, such as particle size and EE, at a significance level of $p<0.05$. *In vitro* studies of the prepared NSs demonstrated promising anticancer activity. The AMY + HGN combination showed synergistic effects versus AMY alone, significantly influencing the MCF-7 cell cycle, producing G1-phase arrest, and reducing cell propagation by flow-cytometry analysis.

Conclusion: The synergistic anticancer activity observed with AMY- and HGN-loaded NSs-combined with their sustained-release properties and cell-cycle modulation in MCF-7 cells-underscores the promise of this formulation as an effective cancer-treatment approach.

Keywords: Nanosponges, cancer, higenamine, synergistic, α-amyrin

INTRODUCTION

Cancer has a significant impact on global mortality, accounting for approximately 1 in every six deaths and affecting almost every household. In 2022, there were 20 million new cases of cancer and 9.7 million deaths globally ascribed to cancer. The World Health Organization projects a 77% increase in the burden of cancer by 2050, which will place additional strain on health systems and communities.[1-6]

***Correspondence:** shailaja.dombeagcop@gmail.com, **ORCID-ID:** orcid.org/0000-0002-4151-1590
Received: 08.08.2024, **Accepted:** 02.06.2025 **Publication Date:** 01.08.2025

Cite this article as: DOMBE SA, SHIROTE PJ. Physicochemical characterization, drug release, stability, and cytotoxicity of cross-linked curdlan-based. Turk J Pharm Sci. 2025;22(3):178-190

Despite these concerning statistics, there is a glimmer of hope. In the last two years, the mortality rate due to cancer has declined according to advancements in understanding tumor biology and the development of improved investigative devices and therapies.[6-7] Currently, mainstream cancer therapies include surgical intervention, radiation, and chemotherapeutic drugs. However, these interventions often harm normal cells, leading to toxicity in patients.[8] While conventional chemotherapy protocols are effective, they are also accompanied by adverse effects that can compromise biological efficacy and patient outcomes.

Exploring the principles of ancient Indian medicine, particularly Ayurveda, unveils a promising path forward. It appears that nature holds a treasure trove of potent components with anti-proliferative and anti-angiogenic properties.[9] Natural products exhibit remarkable chemical versatility and biological specificity, along with reduced toxicity. These characteristics make them valuable contenders for the creation of new and innovative medications.

The modern pharmaceutical market increasingly favors bioactive compounds obtained from natural sources due to concerns about the side effects associated with chemotherapeutic medications. Phytochemicals, valued for their nutritional benefits, not only aid in preventive measures but also hold promise in the treatment of cancer. However, many phytochemicals encounter challenges related to their hydrophilic nature, high molecular weight, and limited absorption through lipid cell membranes, leading to low bioavailability and efficacy. The current landscape of pharmacotherapy relies on traditional dosage forms, which offer therapeutic benefits to a limited extent and thus present significant obstacles in the effective treatment of cancer. As research advances, the exploration of natural compounds brings a renewed sense of optimism in the ongoing battle against this formidable disease.[10]

Alpha-amyrin (AMY) is a pentacyclic triterpene compound with the molecular formula $C_{30}H_{50}O$ isolated from the leaves of *Capparis zeylanica* L. and has reported pharmacological activities such as anti-diabetic, anticancer, anti-inflammatory, antioxidant, and antimicrobial. The molecular weight of AMY is approximately 426.71 g mol^{-1}, and its melting point falls within the range of 252-256 °C. AMY is practically water-insoluble but soluble in various solvents, including ethanol, chloroform, and acetone. Its physical properties present certain challenges-hydrophobia, high molecular weight, and low bioavailability-making it a compelling candidate for formulation development.[11]

Higenamine (HGN) is an isoquinoline derivative isolated from *Annona squamosa* L. it is also called norcoclaurine, a natural compound found in various plants, including *A. squamosa* (sitaphal). It is classified as a β_2-adrenergic receptor agonist, meaning it stimulates β_2-adrenergic receptors in the body. HGN is soluble in polar solvents such as water and ethanol due to its hydrophilic nature.[12]

So far, research has demonstrated the selective cytotoxic activity of AMY-loaded nanocapsules in leukemic cells. This study aims to combine AMY with HGN for breast-cancer treatment, to reduce side effects, enhance cytotoxicity, and improve bioavailability compared to conventional chemotherapy.[13]

Natural-polymer-based nanosystems demonstrate superior drug-loading capabilities compared with other available nanocarriers, effectively addressing issues related to physicochemical properties as well as bioavailability and stability for a wide range of therapeutic agents. Notably, natural polymers such as curdlan, hydroxypropyl cellulose, guar gum, xanthan gum, and ethylcellulose are commonly utilized to facilitate sustained release.[14]

Despite significant advancements in nanotechnology for drug delivery, no previous study has explored the combined application of AMY and HGN in nanosponge (NS)-based systems for cancer treatment. This knowledge gap highlights the novelty and importance of this investigation. The study addresses critical challenges associated with traditional chemotherapy, such as systemic toxicity, low therapeutic index, and the limitations of natural bioactive compounds, including poor solubility and bioavailability. Specifically, this work focuses on AMY and HGN—two phytochemicals known for their potent anticancer properties but whose clinical translation is hindered by these physicochemical constraints. To overcome these barriers, the study proposes the development of a curdlan-based (NS) formulation. Curdlan, a natural polymer, offers biocompatibility and biodegradability, making it an ideal candidate for nanoscale drug-delivery systems aimed at improving the therapeutic efficacy of AMY and HGN against breast cancer (MCF-7 cells).

The curdlan-based NS are designed to enable sustained drug release, reduce systemic side effects, and achieve enhanced therapeutic outcomes. To achieve these objectives, the study systematically explores the role of curdlan polymer composition and stirring rate in the fabrication of NS, assessing their influence on critical parameters such as particle size, encapsulation efficiency (EE), and therapeutic performance. The formulation is characterized and evaluated for its *in vitro* cytotoxicity against MCF-7 cells and its ability to induce cell death through flow-cytometry analysis.The rationale for this approach stems from the need to enhance the delivery, stability, and bioavailability of these compounds while leveraging their synergistic anticancer potential.[14-15] This innovative strategy aims to establish a robust, curdlan-based NS platform that addresses existing limitations in cancer drug delivery while contributing to the advancement of phytochemical-based therapeutics.

MATERIALS AND METHODS

HGN standard was obtained from Sigma-Aldrich (Bangalore, India). Dichloromethane (DCM) was procured from Thermo Fisher, while methanol was sourced from Merck. AMY was purchased from Chem-scene (China). Polyvinyl alcohol from Rankem and toluene from Qualigens (Thermo Fisher Scientific) were used.

Methodology

Preformulation study

Ultraviolet-visible (UV-visible) spectroscopy

To find the absorption maxima of HGN and AMY, standard solutions were individually scanned in a UV spectrophotometer between 200 and 400 nm, with methanol serving as a blank. The wavelength at which the spectra of the two medications overlap is known as the isosbestic point. To generate a calibration curve, working solutions were prepared, and their absorbance at the isosbestic point was measured.

Fourier transform infrared spectroscopy (FTIR)

An analytical method commonly used to identify chemical interactions is FTIR spectroscopy. In this study, the FTIR (Bruker, Germany) was used to determine the infrared spectra of HGN, AMY, curdlan polymer, physical mixture, and the optimized batch. A small quantity of the material was put on the infrared platform, and the spectra were analyzed in the wavelength range between 4000 and 400 cm^{-1}.

Differential scanning calorimetry (DSC)

The thermal behavior and thermotropic properties of the medication were assessed using DSC (SDT Q600 V20.9 Build 20, TA Instruments, New Castle, DE, USA). This method involves measuring the heat flow through the sample and reference under controlled temperature programming. DSC analyses were conducted on HGN, AMY, curdlan polymer, physical mixture, and the optimized batch. A DSC thermogram for the pure drug was obtained by heating five milligrams of the sample at a rate of 10 °C/min in a closed metal pan in a nitrogen environment with an evacuation rate of 20 mL/min. These investigations assisted in determining the thermal behavior of the drug-polymer physical mixture and the optimal batch so that their compatibility could be verified.[15-16]

Formulation and optimization of NS

Optimization of formulation parameters and process factors

A specific formula was chosen for the formulation of NS based on saturation solubility studies. As part of the preparation method optimization, various parameters were adjusted, such as polymer concentration, the stabilizer choice, volume of the aqueous phase, nature of the organic solvent, stirring time, and stirring speed. The resulting NS characteristics were comprehensively evaluated during the formulation optimization process. Different batches were formulated with varying polymer concentrations, each subjected to distinct stirring speeds of 1000, 2000, and 3000 rpm.

Factorial design

The study employed a 3^2 factorial design, where two factors, each with three levels, were investigated. Design Expert®, version 11.0 (Stat-Ease Inc., Minneapolis, MN, USA), was used to create the design. In this study, a 3^2 full factorial design was implemented, focusing on curdlan amounts (X_1) and stirring speed (X_2) chosen as independent variables. The levels of these two factors, with three different levels: low, medium, and high, were established based on a preliminary study conducted before initiating the experimental design. Throughout the study, all other formulation and processing variables remained constant. The response variables selected were particle size (Y_1) and (EE, Y_2). The prepared NS batches were evaluated and characterized across various parameters. Furthermore, the software Design Expert 11.0 advocated for a singular formulation (F10) through a multi-criterion decision strategy to optimize responses targeting various objectives. The optimal values for the variables were ascertained to be X_1 =250 mg and X_2 =1000 rpm; the formulation was counterchecked for correctness by checkpoint analysis.

Preparation of phytochemicals loaded NS

Emulsion solvent diffusion method

Various quantities of polymer can be used to produce NS as shown in Table 1. The dispersing phase, comprising a specified quantity of polyvinyl alcohol, was gently added to 100 mL of water as a continuous phase. The reaction mixture was stirred for two hours at different rpm. The generated NS were recovered by filtering, then dried for 24 hours at 40 °C in the oven. The vacuum desiccators were used to store the dried NS to make sure that any remaining solvents had been eliminated.

Evaluation of phytochemicals loaded NS

Production yield (PY)

PY was calculated using the following formula:

$$PY\ (\%) = \frac{\text{Actual wt of nanosponge}}{\text{Theoretical wt of the drug and polymer}} \times 100$$

Encapsulation efficiency (EE)

The assessment of the drug quantity encapsulated within NS is crucial, as it influences the release mechanism and ultimately the bioavailability. To determine the EE, NS (150 mg) was thawed in methanol, sonicated for 15 minutes, and then centrifuged. The resulting supernatant was filtered, appropriately diluted using pH 6.8 phosphate buffer, and subjected to analysis using a UV spectrophotometer at 219 nm. The EE was determined by the given formula provided below:

$$\%\ EE = \frac{\text{Actual drug content (NS)}}{\text{Theoretical drug taken}} \times 100$$

Scanning electron microscopy

The surface structure and morphology were examined using a scanning electron microscope (S-3400 N type II model, Hitachi Ltd., Tokyo, Japan).

Particle size and polydispersity index (PDI)

The size of AMY-HGN-loaded NS and the PDI (to assess the dispersion of particle size) were determined using dynamic light scattering at 25 °C. This method was conducted using a nanoparticle analyzer (SZ-100) from Horiba Scientific, Japan. The NS dispersion was diluted and placed into the portable measuring cuvette before being inserted into the instrument's cuvette holder for evaluation. Before measurement, any air

Table 1. Composition of nanosponges containing AMY and HGN

Components	F1	F2	F3	F4	F5	F6	F7	F8	F9
Higenamine (Ratio)	1	1	1	1	1	1	1	1	1
α-Amyrin	1	1	1	1	1	1	1	1	1
Curdlan (mg)	250	250	250	500	500	500	750	750	750
Polyvinyl alcohol (mg)	500	500	500	500	500	500	500	500	500
Dichloromethane (mL)	30	30	30	30	30	30	30	30	30
Water (mL)	100	100	100	100	100	100	100	100	100

AMY: Alpha-amyrin, HGN: Higenamine

bubbles in the capillary were removed, and the PDI was then calculated using the following formula:

$$PDI = \frac{\text{Average molecular weight in mass}}{\text{Molecular weight average numbers}}$$

Zeta potential

The measurements were conducted with a separate electrode on the same equipment. To determine the zeta potential, a transparent, single-use zeta cell was filled with 1 mL of NS solution, ensuring the absence of air bubbles. Subsequently, the system was heated to 25 °C by applying an electric field of approximately 15 V/cm, and the outcomes were documented. It is important to note that the stability of the NS preparation increases as the zeta potential becomes more negative.

Drug content

NS was taken (100 mg) and added to 10 mL of phosphate buffer (pH 6.8), then stirred for 30 minutes. Subsequently, the absorbance was measured at the highest wavelength (λmax=219 nm), using spectrophotometry following suitable dilution.

In vitro dissolution study

Dissolution studies are conducted to investigate the probable impact of formulation and process variables on the bioavailability of a medication. In this study, a paddle-shaped USP Type-II dissolution apparatus was used to assess the *in vitro* release of NS. The NS was placed into dialysis bags, followed by immersion in phosphate buffer (pH 6.8), with 900 mL serving as dissolution media. The system was kept at 37.5 °C with stirring at 100 rpm. At regular intervals, 5 mL samples were withdrawn up to 12 hours and were replaced with the same amount of the dissolution media. The absorbance of these samples was taken spectrophotometrically at 219 nm.

In vitro drug release kinetics

Plotting the following kinetic models-zero order, first order, Higuchi equations, and Hixson-Crowell, using the data gathered from *in vitro* release tests, allowed the determination of NS drug release kinetics. The Korsmeyer-Peppas equation was utilized to determine the drug release mechanism.[16,17]

MTT assay

The MCF-7 cell from the Biocyte Institute of Research & Development (Sangli, India) was cultured in DMEM-F12 medium augmented with insulin (10 µg/mL), hydrocortisone (0.5 µg/mL), and human epidermal growth factor (20 ng/mL). All culture media were supplemented with high glucose DMEM (catalog number: 11965-092), Antibiotic-Antimycotic 100X solution (Thermo Fisher Scientific, catalog number: 15240062), and fetal bovine serum (FBS) from Gibco (catalog number: 10270106). The cells were initially cultured at a concentration of 1×10^4 cells/mL for 24 hours at 37 °C with 5% CO^2. Subsequently, 104 cells per well were seeded in a 96-well plate, with 70 µl of culture medium, and 100 µl of compounds at concentrations of 10, 40, and 100 µg. Control wells contained cells with 0.2% dimethyl sulfoxide (DMSO) in phosphate-buffered saline (PBS). Following another 24-hour incubation, MTT reagent was added to evaluate cell viability by forming formazan crystals from viable cells. The absorbance at 570 nm was measured after adding DMSO to dissolve the formazan. The percentage of cell growth inhibition was calculated, and the IC_{50} value was determined using 5-Fluorouracil as a positive control.

Apoptosis study by Fluorescence microscopy

A common method for the qualitative assessment of apoptosis at the nuclear level involves using the fluorescent dye 4′,6-diamidino-2-phenylindole dichloride (DAPI), which binds to DNA and can be visualized under a fluorescence microscope. In this study, we employed a DAPI staining protocol as previously described. In brief, MCF-7 cells were seeded onto 6-well plates at a density of 5 × 10^5 cells per well, and they were left to adhere and proliferate for a full day. The cells were treated with 5-FU as the standard treatment. The cells were also treated separately using the optimized formulation. Then, they were washed with PBS, followed by being fixed with 10% formaldehyde. After that, the cells were permeabilized for 15 minutes using Triton X-100. Following additional washes, the cells were stained with DAPI for 5 minutes. Apoptotic nuclei, characterized by fragmentation or condensation, were visualized using a fluorescence microscope (Micron India). Untreated cells were used as the control in this experiment.

Cell cycle analysis

The distribution of cell cycles was assessed by flow cytometry following DAPI staining. MCF-7 cells were exposed to the optimized formulation or an equivalent amount of DMSO as a control for 24 hours. Subsequently, floating cells were gathered, while adherent cells underwent trypsinization, followed by washing with PBS containing 5% FBS, and centrifugation at

1100 g for 10 minutes. The resulting cell pellets were then suspended in 500 µl of PBS with 5% FBS, centrifuged at 200 g for 7 minutes at 4 ˚C, and stained with a solution containing PI, Triton X-100, sodium citrate, and RNase. Following an hour of incubation at 4 ˚C in the dark, flow cytometric analysis was carried out using a FACSCalibur instrument (BD Biosciences, USA).[18-20]

Stability studies

Following International Council for Harmonisation of Technical Requirements for Pharmaceuticals for Human Use guidelines, the stability testing involved subjecting the samples to conditions of 40 ˚C ± 2 ˚C and 75% relative humidity (RH) ± 5% RH for a duration of six months. Following the standard protocol, the samples were assessed at intervals of 0, 3, and 6 months. These accelerated stability tests were conducted on the ultimate optimized formulation.[21,22]

Statistical analysis

Regression analysis was performed to determine the comparative effect of the independent variables, X1 (polymer concentration) and X2 (stirring rate), on the dependent variables, R1 (particle size) and R2 (EE). The final regression equations were presented in terms of coded factors. These equations help quantify the impact of the independent variables on the dependent variables. The statistical significance of the coefficients in the equations demonstrates the reliability of the results.[22]

RESULTS

Preformulation studies

Ultraviolet-visible (UV-visible) spectroscopy

HGN and AMY exhibited (λ max) of 254 nm and 208 nm, respectively, when dissolved in methanol. Figure 1 displays an overlay plot of these two drugs. The isosbestic point of the two drugs was found to be 219 nm. Calibration curves and graphs for a mixture of HGN and AMY were constructed using methanol. These exhibited a regression coefficient of 0.998, with a slope value of 0.143 and a Y-intercept value of 0.0049.

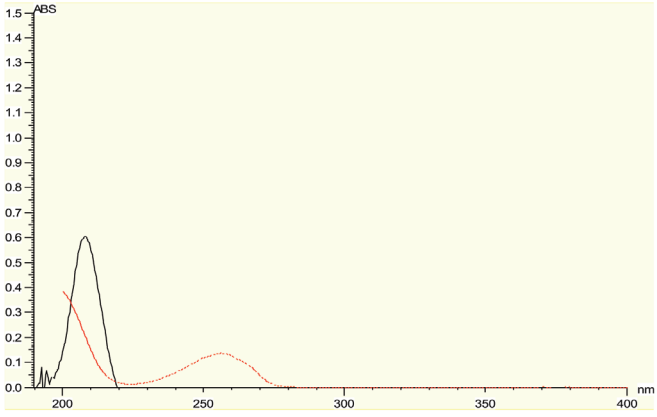

Figure 1. Overlay spectrum of HGN and AMY mixture in methanol
HGN: Higenamine, AMY: alpha-amyrin, ABS: Absorption,

This suggests a linear relationship between concentration and absorbance within the range of 10-60 µg/mL for the HGN and AMY in methanol.

Fourier transforms infrared spectroscopy (FTIR)

FTIR spectroscopy was used to capture the infrared spectrum of HGN and AMY, with the findings presented in Figure 2. The FT-IR spectrum displayed all the characteristic IR peaks corresponding to the functional groups associated with HGN and AMY in the drug mixture and the optimized formulation, as illustrated in Table 2.

DSC analysis

The thermogram of HGN exhibited two endothermic peaks, *i.e.*, 98.94 ˚C and another at 246.07 ˚C, which may represent the loss of water or solvent molecules and the melting of the sample, respectively. The melting point of the sample is reported to be 258-260 ˚C, which is consistent with the observed peak at 246.07 ˚C. The thermogram of AMY showed a peak at 170.67 ˚C, representing a melting point (theoretically 186 ˚C). The polymer can be accredited with its peak melting point at 282.77 ˚C. The physical mixture exhibited the endothermic peak at 304.34 ˚C for curdlan polymer. This DSC analysis indicated that

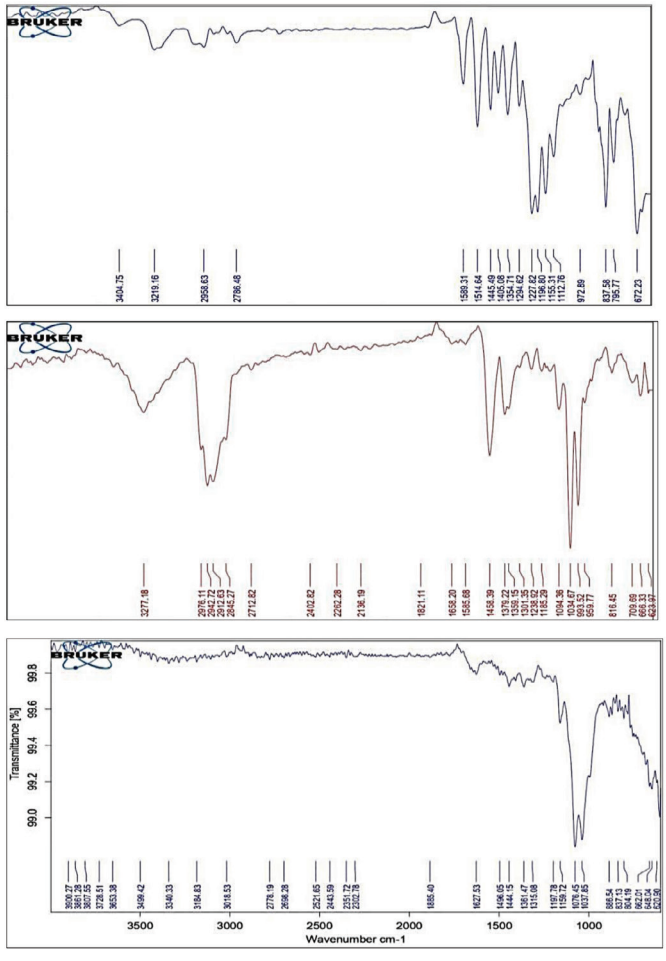

Figure 2. FTIR spectrum of (A) HGN, (B) AMY, (C) optimized formulation
FTIR: Fourier transform infrared spectroscopy, HGN: Higenamine, AMY: alpha-amyrin

Table 2. Interpretation of FT-IR spectrum of HGN and AMY physical mixture

Sr. no.	Frequency (cm^{-1})	Peak observed	Interpretation
1	3550-3220	3222,3217.8	Phenol O-H Stretch
2	3000-2850	2943,2958	Alkane C-H Stretch
3	1480-1350	1357.93,1411,1447	Aromatic C=C stretching vibrations
4	3500-3300	3184.83	Amine N-H Stretch
5	1360-1080	1315.08	Amine C-N Stretch
6	1640-1550	1599.04	Amide N-H bending
7	1000-650	885.54	Alkene=C-H bending

Sr. no.: Serial number, FT-IR: Fourier transform infrared spectroscopy, HGN: Higanamine, AMY: alpha-amyrin

no noteworthy change was perceived in the melting points of both drugs in combination. The thermogram of DSC is shown in Figure 3.

Formulation and optimization of NS

Compatibility study for Nanosponges

FT-IR analysis

The spectra of HGN and AMY, as well as the physical mixture, were analyzed. The functional groups identified in the physical mixture of drugs and polymer were found to align with the peaks observed for the pure drugs. Notably, Figure 2 demonstrates the significant peaks of the drug mixture-including 3018.53 cm-1 for Alkane C-H stretching, 837.13 cm-1 for alkene C-H bending, 1361.47 cm-1 for amine C-N-stretching, and 1627.53 cm-1 for amide N-H bending, in the FT-IR spectra of the physical mixture.

DSC analysis

The DSC Thermograms of HGN and AMY, as well as the drug-polymer physical mixture, are presented in Figure 3. The drug mixture displayed endothermic peaks of HGN and alpha-amyrin at 246.07 ˚C and 170.67 ˚C, respectively. In contrast, the physical mixture of drugs and the polymer demonstrated an endothermic peak at 304.34 ˚C for the curdlan polymer.

Evaluation alpha-amyrin and higenamine loaded NS

Production yield and EE

The production yields of the prepared formulations varied between 41.53% and 70.36%. The proportion of drug to polymer was identified as having a crucial role in determining production yield, indicating that increased polymer concentrations resulted in higher yields. On the other hand, the EE of all formulations ranged from 59.23% to 81.79% as shown in Table 3.

Particle size and PDI

Measurements were made of the formulation of NS particle size analysis as reported in Table 4. The results indicate that the particle size of the various formulations ranged from 241.3 nm to 622.2 nm. The PDI across the formulations ranged from 0.382 to 0.960, which suggests a considerable variance in particle size distribution. Notably, the relatively high PDI values suggest a range in the distribution of particle sizes, with some formulations exhibiting a more uniform distribution than others.

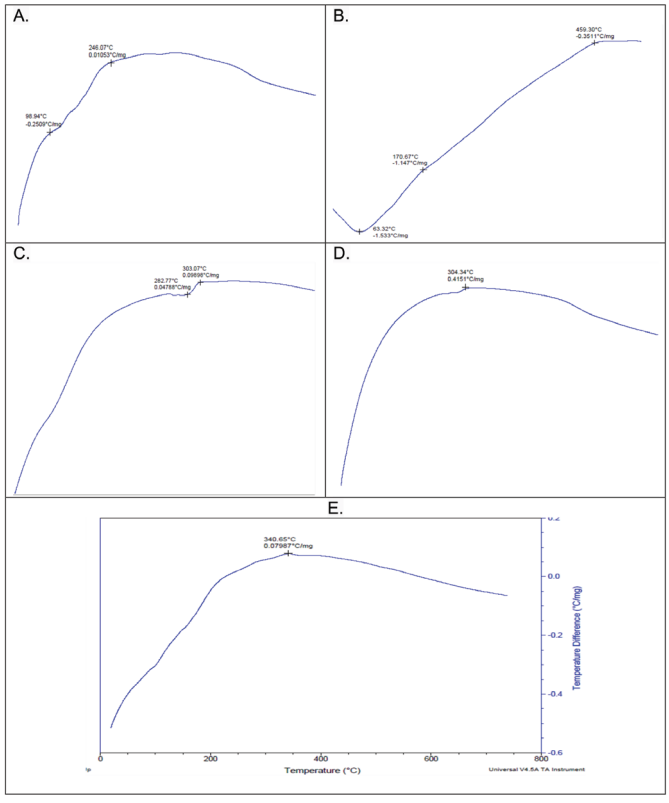

Figure 3. DSC thermogram of (A) HGN, (B) AMY, (C) polymer, (D) physical mixture, (E) optimized formulation

DSC: Differential scanning colorimetry, HGN: Higenamine, AMY:alpha-Amyrin

This might have implications for the stability and performance of these formulations, potentially influencing their suitability for specific applications and delivery systems.

Zeta potential

The zeta potential values of formulations ranged from -5.5 mV to -23.3 mV, a range that is crucial for maintaining physical stability among nanoparticles (NS) by promoting electrostatic repulsion and preventing aggregation. Furthermore, the reduction in particle size results in an increased surface area,

which in turn contributes to higher zeta potential values, as observed in Table 5.

In vitro drug release studies

NS were produced and evaluated, utilising an emulsion solvent diffusion method, providing several key outcomes for the effective creation of NS. The *in vitro* drug release profile ranged from 79.60 to 91.58% CDR for 12 hours, which revealed that the formulation with a higher coded value for the polymer and a lower coded value for stirring rate exhibited the highest *in vitro* drug release compared to the other formulations (Figure 4) as detailed in Table 6.

Experimental design for NS formulations

The outcomes obtained for selected software responses are detailed in Table 7. The particle size of all runs ranged from 241.3 nm to 622.2 nm, and entrapment efficiency (%) was observed ranging from 79.60% to 91.80%.

Table 3. Data for production yield and EE for NS formulation

Sr. no.	Batch	PY (%)	EE (%)
1	F1	45.60±0.75	62.00±0.81
2	F2	47.43±0.50	60.00±1.63
3	F3	41.53±0.55	65.45±0.41
4	F4	51.26±0.57	66.00±0.81
5	F5	55.70±0.36	80.24±0.50
6	F6	50.51±0.42	79.63±1.73
7	F7	70.63±0.49	81.79±0.57
8	F8	66.63±0.54	59.23±0.32
9	F9	62.83±0.60	69.63±1.73

Data are mean values (n=3) ± SD. SD: Standard deviation, Sr. no.: Serial number, PY: Production yield, EE: Entrapment efficiency

Table 4. Particle size and PDI of NS formulation

Sr. no.	Batches	Particle size (nm)	PDI
1	F1	280.9±0.82	0.496±0.0005
2	F2	290.7±0.12	0.381±0.0630
3	F3	389.9±0.91	0.557±0.0035
4	F4	420.1±0.58	0.960±0.0026
5	F5	241.3±0.28	0.559±0.0024
6	F6	349.5±0.89	0.589±0.0026
7	F7	502.3±0.42	0.493±0.0024
8	F8	613.5±0.41	0.596±0.0008
9	F9	622.2±0.71	0.685±0.0670

Data are mean values (n=3) ± SD. SD: Standard deviation, Sr. no.: Serial number, PDI: Polydispersity index

Regression analysis

The regression equations represented the comparative effect of the independent variables X1: polymer concentration (mg) and X2: stirring rate on dependent variables R1: particle size (nm) and R2: EE (%).

The final equation in coded factors terms

The equation for response R1 has shown that both factors have a significant positive effect on the particle size of NS formulations.

$$R1 = +412.27+129.43X1+26.38X2 \quad (1)$$

The equation for response R2 has shown that factor X1 has a positive effect, whereas factor X2 has a negative effect on EE of NS formulations.

$$R2 = +69.33 +4.69\ X1 - 16.38\ X2 \quad (2)$$

The experimental runs of the nine trials are listed in Table 7. The effects of the main factors on the formulation responses are noted in the regression equations. An increase in the independent variable X1 led to an increase in particle size and EE. While an increase in X2 resulted in a larger particle size, it caused a decrease in EE.

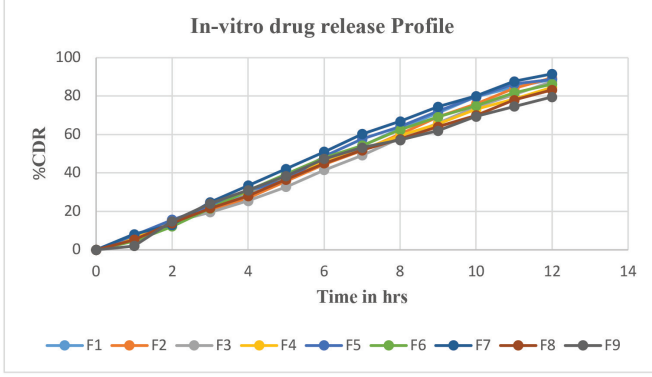

Figure 4. *In vitro* drug release profiles of F1 to F9 batches

Table 5. Zeta potential of NS formulation

Sr. no.	Batch code	Zeta potential (mV)
1	F1	-5.5±0.32
2	F2	- 5.6±0.22
3	F3	-11±0.42
4	F4	-23.3±0.26
5	F5	-13±0.39
6	F6	-15±0.20
7	F7	-6.4±0.25
8	F8	-10.5±0.31
9	F9	-12.7±0.28

Data are mean values (n=3) ± SD. NS: Nanosponge, SD: Standard deviation, Sr. no.: Serial number

Response-surface analysis

The primary objective of optimization is to determine the most effective levels of the variables that impact the process, enabling the smooth and consistent production of a product with desired attributes. The effects of various independent variables on the dependent variables were expressed using 3D graphics. The polymer concentration and stirring speed had a significant effect on particle size, whereas polymer concentration had a significant impact on entrapment efficiency. The response surface graphs the most statistically significant variables for the evaluated responses as shown in Figure 5.

Analysis of variance (ANOVA)

The model was established for all dependent variables, such as particle size and entrapment efficiency, at a significance level of $p<0.05$. The linear model showed the best fit for both responses.

Checkpoint analysis and optimization of design

Through the Design of Experiments (DOE) methodology to optimize responses targeting various objectives, the software Design Expert 11.0 advocated for a singular formulation (F10) through a multi-criterion decision strategy. The optimal values for the variables were ascertained to be X1=250 mg and X2 =1000 rpm. The final formulation was developed by applying optimal factor values and subsequently evaluated for particle size and entrapment efficiency. The optimized formulation, represented by F10, exhibited a particle size measuring 280.9 nm alongside an entrapment efficiency of 63.00%. Comparing the predicted and observed outcomes revealed a desirability

Table 6. *In vitro* drug release profiles of F1 to F9 batches

Time (Hours)	% CDR								
	F1	F2	F3	F4	F5	F6	F7	F8	F9
0	0	0	0	0	0	0	0	0	0
1	5.50	6.80	7.60	6.20	7.56	4.53	8.19	5.20	2.06
2	14.33	15.56	14.55	14.85	15.6	12.16	13.03	13.90	14.88
3	22.66	20.15	19.56	23.45	22.63	21.60	24.83	21.70	24.15
4	29.63	27.00	25.45	30.12	30.89	30.90	33.5	28.00	31.02
5	38.23	35.78	32.74	38.40	36.45	39.35	42.16	36.57	38.41
6	46.06	44.56	41.58	45.61	48.56	47.88	51.03	45.00	47.28
7	54.00	51.74	49.12	52.19	57.65	54.26	60.23	51.79	53.21
8	63.23	60.12	58.07	59.46	64.23	62.45	66.85	57.60	57.18
9	71.28	69.24	66.05	65.58	72.24	69.12	74.52	64.12	62.00
10	79.55	76.00	74.24	73.12	79.57	75.00	80.05	70.00	69.35
11	84.72	83.99	80.70	80.40	84.26	81.76	87.69	77.91	74.59
12	88.69	86.56	87.21	88.58	87.69	86.26	91.58	83.26	79.60

CDR: Cummulative drug release

Table 7. 3^2 full factorial design layout and responses noted for NS formulation

Trial	Polymer conc (X1)	Stirring time (X2)	Particle size Y1	Entrapment efficiency Y2
1	250	1000	280.9±0.82	62.00±0.81
2	250	2000	290.7±0.12	60.00±1.63
3	250	3000	389.9±0.91	65.45±0.41
4	500	1000	420.1±0.58	66.00±0.81
5	500	2000	241.3±0.28	80.24±0.50
6	500	3000	349.5±0.89	79.63±1.73
7	750	1000	502.3±0.42	81.79±0.57
8	750	2000	613.5±0.41	59.23±0.32
9	750	3000	622.2±0.71	69.63±1.73

Data are mean values (n=3) ± SD. NS: Nanosponge, SD: Standard deviation

value of 0.656 with minimal relative errors, endorsing the dependability of the optimization process. Additionally, the strong coherence between the projected and observed values was evidenced in Table 8, underscoring the efficiency and accuracy of the optimization process employed. Factors X1 and X2, determined as 250 mg and 1000 rpm, respectively, were recognized as the optimum parameters for the NS drug delivery system.

Characterization of optimized NS formulation

Scanning electron microscopy (SEM)

SEM analysis was conducted on the prepared NS to examine their morphology and surface texture. The NS were found to be approximately spherical, displaying an uneven surface and a porous, spongy nature, as depicted in Figure 6.

Particle size analysis, zeta potential measurement

The measured particle size closely matched the predicted value obtained from the DOE. Table 8 illustrates that the predicted and observed particle size values for the NS were similar, with a residual value of 24.44 existing between them. A reduction in particle size enhances the interfacial area available for drug diffusion, potentially leading to improved drug release. Additionally, the narrow size distribution helped increase bioavailability.

The zeta potential of the NS formulation was determined to be -5.8 mV, contributing to the physical stability of the NS particles through electrostatic repulsion, thereby preventing aggregation. Moreover, the decrease in particle size resulted in an increased surface area, leading to a higher zeta potential. A zeta potential of -5.8 mV signifies a slight negative charge on the particle surface, indicating a tendency for repulsion between particles and supporting the stability of the colloidal system.

Entrapment efficiency

The achieved EE closely aligned with the predicted value derived from the DOE. As detailed in Table 8, the predicted and observed values of drug entrapment in the NS were nearly identical, with a residual value of 6.33.

FT-IR analysis of NS

FT-IR spectroscopy was conducted on the optimized formulation to confirm the entrapment of the drug mixture within NS. The absence of major peaks associated with the drug mix, such as phenolic OH group stretch (3510.56 cm-1), amine N-H stretch (3112.26 cm-1), and alkene=C-H bonding (740.69 cm-1), in the NS formulation spectra, confirms the drug mixture's entrapment within the polymer system of NS in Figure 2. Furthermore, characteristic peaks present in the pure drug mix and the drug and polymer physical mixture, including alkane C-H stretch, alkene C-H bending, amine C-N stretch, and amide N-H bending, were found in the optimized formulation, indicating the presence of the drug in the NS.

DSC analysis of NS

The DSC thermogram of the optimized NS formulation, depicted in Figure 3, revealed an endothermic peak at 340.03 °C, indicating the presence of Curdlan polymer. The absence of peaks related

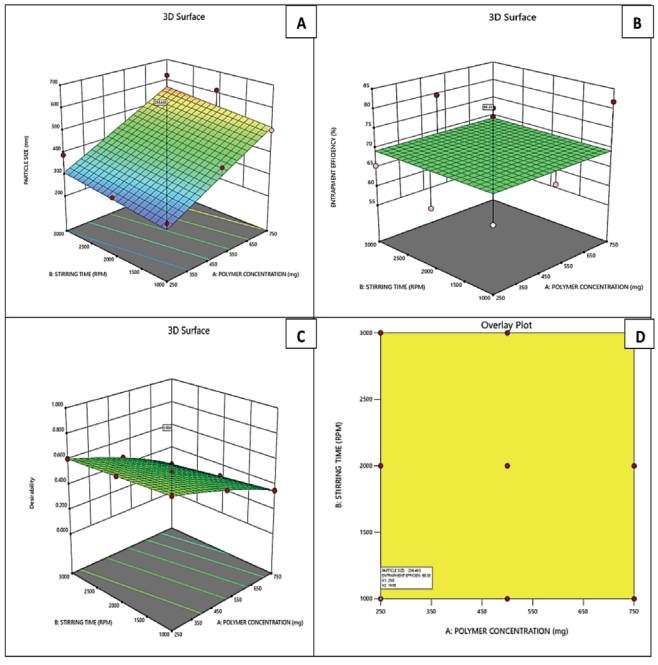

Figure 5. (A) 3D surface plot for particle size, (B) entrapment efficiency, (C) Desirability plot, (D) Overlay plot for polymer concentration and stirring rate

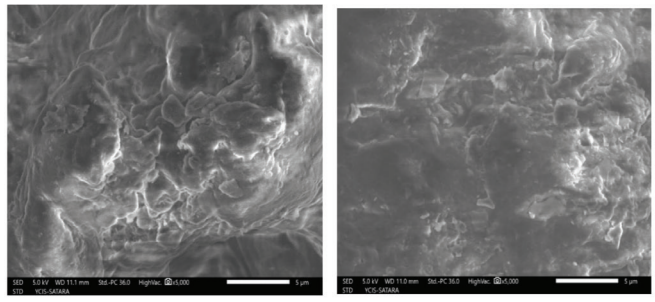

Figure 6. SEM micrograph of optimized formulation
SEM: Scanning electron microscopy

Table 8. Check point analysis of optimized NS formulation F10

Response	Expected	Observed	Residual	Desirability
Particle size (nm)	256.46	280.9	24.44	0.656
EE (%)	69.33	63	6.33	0.656

NS:Nanosponge, EE: Entrapment Efficiency

to drugs indicated that the drug mixture is encapsulated within the polymer system, demonstrating its compatibility.

Drug release kinetic study of optimized formulation

For the assessment of release kinetics, the drug release data underwent analysis using various kinetic equations. This analysis involved evaluating key parameters, correlation coefficient (R), and release exponent (n)-to explore the release mechanism. Table 9 presents the correlation coefficient (R) for the optimized formulation.

The model that gave a high 'R' value was considered the best fit for the release data. The Korsmeyer-Peppas model best described the sustained release of the optimized formulation: the diffusion exponent (n) value. From the result, the best fit model for optimized formulation is zero zero-order model (Figure 7).

Super Case II transport specifically refers to the situation where the release exponent (n=0.9210) is greater than 0.89. In this scenario, the drug release mechanism is considered to be more dominated by polymer relaxation or erosion compared to the standard "anomalous transport" in the range of 0.45 to 0.89. It implies that the release kinetics are significantly influenced by the swelling, relaxation, or erosion of the polymeric matrix.

MTT assay

Prior research has highlighted the anticancer properties of *Annona squamosa* L. the leaves extract. Hence, this study seeks to explore the anticancer activity of isolated HGN specifically on breast cancer cells.

Different doses ranging from 10 µg to 100 µg of various compounds were evaluated for their anti-tumor effects on the MCF-7 cell line. Notably, HGN demonstrated an IC_{50} value of 42.39 µg/mL in MCF-7 breast cancer cells, exceeding the IC_{50} of 5-fluorouracil at 39.22 µg/mL, indicating promising activity compared to the standard compound, as depicted in Figure 8. Similarly, AMY derived from *Capparis zeylanica* L. was evaluated at different doses (ranging from 10 µg to 100 µg) for its antitumor activity against the MCF-7 cell line. An IC_{50} value of 34.54 µg/mL for AMY was observed in MCF-7 breast cancer cells. AMY outperformed 5-fluorouracil, which has an IC_{50} of 39.22 µg/mL. The samples demonstrated noteworthy activity compared to the standard compound, as illustrated in Figure 9. Moreover, the combination of both HGN and AMY yielded an IC_{50} value of 43.03 µg/mL, whereas the optimized NS formulation showed an IC_{50} value of 33.71 µg/mL.

Apoptosis analysis

In the study to evaluate the apoptotic effects of the optimized batch, DAPI staining was conducted. The results from the control group in Figure 10A revealed normal nuclear morphology with intact and evenly distributed chromatin. Figure 10B displayed significant DNA alterations in cells treated with fluorouracil, which indicates apoptosis or cell death, characterized by condensed or fragmented nuclei. Moreover, changes in nuclear architecture, such as membrane blebbing and apoptotic body formation, were observed, which is characteristic of apoptotic cells. The optimized formulation depicted in Figure 10C demonstrated a notable decrease in the MCF-7 cell population, primarily showing mitotic morphology suggestive of effective G2/M cell cycle arrest. The images exhibited highly fragmented cell nuclei, substantial cell loss, and extensive cellular damage.

Table 9. Release kinetics of optimized formulation

Model		Formulation code
Zero order	R^2	0.9981
First order	R^2	0.9877
Higuchi model	R^2	0.8925
Hixson-Crowell	R^2	0.9929
Korsmeyer Peppas	R^2	0.9618
Best fit model	Zero order model	

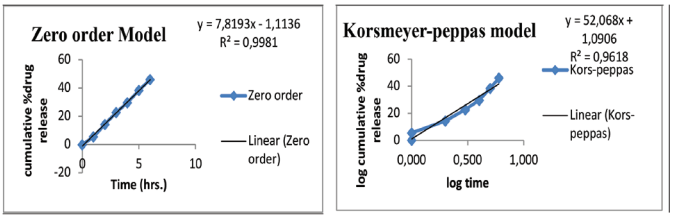

Figure 7. Release kinetics graph of optimized formulation

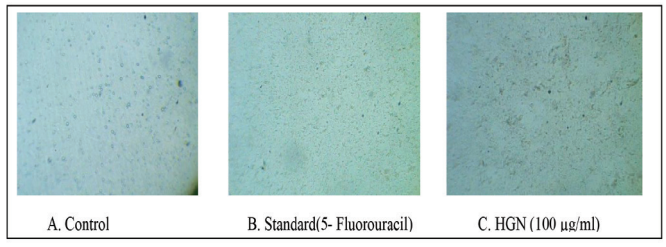

Figure 8. Cell line study with MCF-7 breast cancer cell line (A) control, (B) standard, (C) HGN

MCF: Michigan Cancer Foundation, HGN: Higenamine

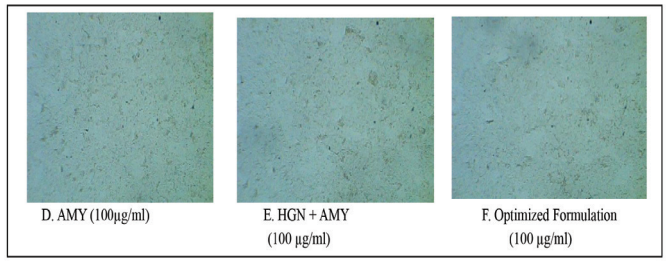

Figure 9. Cell line study with MCF-7 breast cancer cell line (D) AMY, (E) HGN + AMY, (F) optimized formulation

MCF: Michigan Cancer Foundation, AMY: alpha-amyrin, HGN: Higenamine

Cell cycle analysis

Figure 11A illustrates the distribution of cells treated with the optimized formulation based on granularity and APC fluorescence. The percentages of cells in different cell cycle phases were observed as follows: G0 (24.56%), G1 (48.21%), S (25.26%), G2 (15.36%), and M (3.25%). A red box marked with a star highlights a region with no events (0%). Figure 11B demonstrates a clear correlation between cell size and granularity, with the majority of cells (88%) falling within the red-boxed region, indicating a specific population of cells with consistent size and granularity properties. Figures 11C and 11D show the relationship between cell size (diameter) and APC fluorescence. In these plots, only a small number of events were detected in the red-boxed region (4.33 counts in plot C and 3.89 counts in plot D), which represents near 0% of the total events.

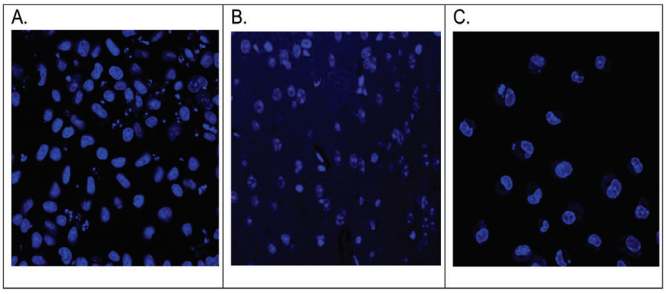

Figure 10. Nuclear morphology of MCF-7 cells after DAPI staining. (A) control, (B) Std. 5-FU, (C) optimized formulation

MCF: Michigan Cancer Foundation, DAPI: 4',6-diamidino-2-phenylindole, Std.: Standard, 5-FU: 5-Fluorouracil

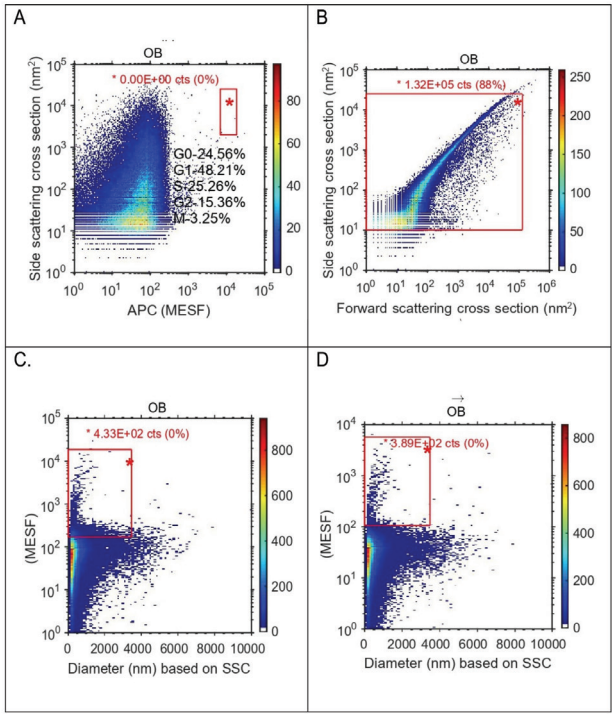

Figure 11. Flow cytometry analysis of optimized formulation with following plots (A) side scattering cross section vs. APC (MESF), (B) side scattering cross section vs. forward scattering cross section, (C) diameter (nm) based on SSC vs. APC (MESF), (D) diameter (nm) based on SSC vs. APC (MESF). Colour Scale: The colour scale on the right indicates the density of cells, with blue representing lower density and red representing higher density

APC: Allophycocyanin, MESF: Molecules of equivalent soluble fluorochrome, SSC: Side scattering cross, OB: Optical block

Stability studies

The stability of the optimized formulation was investigated in accordance with ICH guidelines, evaluating parameters such as drug content and *in vitro* drug release. The outcomes of these investigations are outlined in Table 10. The results indicated that there was no substantial change in the parameters mentioned when subjected to increased temperature and humidity during the stability assessments.

DISCUSSION

The preformulation studies and formulation optimization for the NS loaded with AMY and HGN yield results that provide valuable insights into the physicochemical properties and performance of the developed formulations.

The UV-Visible spectroscopy analysis established the λ max values for HGN and AMY, enabling reliable quantification. Crucial for stability, FTIR spectra confirmed the compatibility between the drug mixture and the polymer, as no interactions were observed. Additionally, DSC analysis showed no significant interactions affecting melting points, underlining the stability of the drug-polymer system and affirming the compatibility of the drug mixture with the polymer.

Variations in production yields and EE were observed based on the drug-to-polymer ratio. Particle size analysis revealed differences in size distribution impacting formulation stability. Negative zeta potential values indicated enhanced stability and minimized aggregation in the NS formulation. *In vitro* drug release profiles highlighted parameter-dependent variations, with optimization potential for improved therapeutic effectiveness.

The experimental design outcomes showcased consistent particle size and EE across formulations, providing a comprehensive overview of the formulation characteristics and highlighting the importance of controlling parameters for desired drug release behavior and efficacy.

Analysis of the SEM micrographs indicated the presence of numerous fine surface voids on the formed NS, presumably attributed to solvent diffusion. Additionally, no residual or intact drug crystals were observed on the NS surface, suggesting the formation of an NS matrix through the interaction of the

Table 10. Stability studies for optimized formulation

Time (Months)	Drug content (%)	*In vitro* drug release (%)
0	81.79±0.68	89.69±0.23
3	81.74±0.99	89.70±0.34
6	81.76±0.78	89.59±0.40

Data are mean values (n=3) ± SD. SD: Standard deviation

drug with the polymer. The FT-IR spectroscopy analysis of the optimized formulation verified the successful entrapment of the drug mixture within the NS. It was validated that the drug mixture had been effectively encapsulated within the polymer structure of the NS. In addition, the presence of characteristic peaks specific to the pure drug mix and the physical mixture of the drug and polymer in the optimized formulation further supported the presence of the drug within the NS matrix in the DSC study. From the result of release kinetics, the best-fit model for the optimized formulation is the zero-order model. The release kinetics are significantly influenced by the swelling, relaxation, or erosion of the polymeric matrix.

The MTT analysis indicated a synergistic effect of HGN and AMY in their anticancer activity, enhanced by their encapsulation into the NS formulation, which promotes increased bioavailability. DAPI staining analysis demonstrated that the optimized formulation induced apoptotic effects on MCF-7 cells, evidenced by DNA alterations, membrane blebbing, apoptotic body formation, and effective G2/M cell cycle arrest, showcasing the formulation's potential for targeted cancer therapy through apoptosis induction and cell cycle modulation.

The cell cycle analysis results offer a comprehensive view of the distribution patterns and characteristics of cells treated with the optimized formulation, shedding light on the formulation's impact on cell cycle progression and highlighting the complexity of cellular responses to the treatment. Consequently, the findings from the stability studies validate that the developed formulation is minimally affected by elevated humidity and temperature.

Overall, the combined results offer a holistic understanding of the physicochemical characteristics, compatibility, stability, and performance of the alpha-amyrin-loaded higenamine-loaded NS formulations, forming a solid foundation for further development and optimization in pharmaceutical applications.

CONCLUSION

Natural polymer-based NS comprising AMY and HGN proved successful in a meticulous 32 full factorial design, with batch F10 serving as their optimal batch. These NS demonstrated superior performance, particularly in their remarkable ability to exhibit enhanced therapeutic effects for combating cancer, offering sustained drug release extending up to 12 hours. *In vitro* studies further illuminated the potential of NS in cancer treatment, marking it as a beacon of promise in the realm of carriers. The development of NS is tailored for breast cancer treatment. Key components like curdlan and DCM were used in the formulation process, with varying polymer concentrations to obtain different NS types. Optimization through a factorial design study identified the ideal combination for results. The NS exhibited controlled drug release patterns, confirmed by a zero-order kinetic model, highlighting consistent release rates. Testing on MCF-7 cell lines, stability assessments, and the inclusion of AMY and HGN in the NS all showcased enhanced anticancer effects and sustained release benefits. Flow cytometry results indicated a significant impact on MCF-7 cell cycles, including cell cycle arrest in the G1 phase and decreased proliferation, underscoring the potential of this NS combination as an innovative and efficient cancer treatment.

Ethics

Ethics Committee Approval: Not required.

Informed Consent: Not required.

Footnotes

Authorship Contributions

Concept: S.A.D., Design: S.A.D., Data Collection or Processing: S.A.D., Analysis or Interpretation: S.A.D., Literature Search: P.S.J., Writing: P.S.J.

Conflict of Interest: The authors declare no conflicts of interest.

Financial Disclosure: The authors declared that this study received no financial support.

REFERENCES

1. Devendra Prajapati, Arindam Chatterjee, Mayank Bansal, Saurabh Pandey. Formulation and evaluation Tolbutamide liposomes for a sustained drug delivery system. J Biomed Pharma Res. 2022;11:16-27.
2. Ali MR, Osmani, Thirumaleshwar S, Rohit R, Bhosale, Parthasarathi K. Nanosponges: The spanking accession in drug delivery - an updated comprehensive review. Der Pharmacia Sinica. 2014;5:7-21.
3. Penjuri SCB, Ravouru N, Damineni S, BNS S, Poreddy SR. Formulation and evaluation of Lansoprazole loaded nanosponges. Turk J Pharm Sci. 2016;13:304-310.
4. SG V, Vaishnav GA, Joshi AS, Girbane YR. Preparation and *in-vitro* assessment of Tolbutamide loaded nanosponges. Ind J Res Methods Pharm Sci. 2022;1:15-20.
5. Iriventi P, Gupta NV, Osmani RAM, Balamuralidhara V. Design & development of nanosponge loaded topical gel of curcumin and caffeine mixture for augmented treatment of psoriasis. DARU J Pharma Sci. 2020;28:489-506.
6. Sathishkumar K, Chaturvedi M, Das P, Stephen S, Mathur P. Cancer incidence estimates for 2022 & projection for 2025: Result from National Cancer Registry Programme, India. Indian J Med Res. 2022;156:598-607.
7. Mizrahy S, Hazan-Halevy I, Landesman-Milo D, Ng BD, Peer D. Advanced strategies in immune modulation of cancer using lipid-based nanoparticles. Front Immunol. 2017;8:69.
8. Lefranc F, Tabanca N, Kiss R. Assessing the anticancer effects associated with food products and/or nutraceuticals using *in vitro* and *in vivo* preclinical development-related pharmacological tests. Semin Cancer Biol. 2017;46:14-32.
9. Choudhari AS, Mandave PC, Deshpande M, Ranjekar P, Prakash O. Phytochemicals in cancer treatment: from preclinical studies to clinical practice. Front Pharmacol. 2020;10:1614.
10. Dombe SA, Shirote PJ. Phytonutraceuticals in cancer prevention and therapeutics. Curr Nutr Food Sci. 2023;19:209-228.
11. Kim SS, Rait A, Kim E, DeMarco J, Pirollo KF, Chang EH. Encapsulation of temozolomide in a tumor-targeting nanocomplex enhances anticancer efficacy and reduces toxicity in a mouse model of glioblastoma. Cancer Lett. 2015;369:250-258.

12. Dombe SA, Shirote PJ. Isolation, *in-silico* studies, and biological evaluation of higenamine from *Annona squamosa* L. against breast cancer. Int J Pharma Qual. 2023;14:1039-1047.
13. SF Neto, AL Prada, LDR Achod, HFV Torquato, CS Lima, EJ Paredes-Gamero, MOS de Moraes, ES Lima, EH Sosa, TP de Souza, JRR Amado. α-amyrin-loaded nanocapsules produce selective cytotoxic activity in leukemic cells. Biomed Pharmacother, 2021;139:111656.
14. Dhimmar B, Pokale R, Rahamathulla M, Hani U, Alshahrani MY, Alshehri S, Shakeel F, Alam P, Osmani RAM, Patil AB. Newfangled topical film-forming solution for facilitated antifungal therapy: design, development, characterization, and *in vitro* evaluation. Polymers (Basel). 2023;15:1003.
15. Darandale SS, Vavia PR. Cyclodextrin-based nanosponges of curcumin: formulation and physicochemical characterization. J Incl Phenom Macrocycl Chem. 2013;75:315–322.
16. Dingwoke E, Felix SY. Development and evaluation of nanosponges loaded extended release tablets of lansoprazole. Univ J Pharma Res. 2019;4.
17. Osmani RAM, Kulkarni PK, Shanmuganathan S, Hani U, Srivastava A, Prerana M, Shinde CG, Bhosale RR. A 3^2 full factorial design for development and characterization of a nanosponge-based intravaginal in situ gelling system for vulvovaginal candidiasis. RSC Adv. 2016;6:18737-18750.
18. Anwer MK, Fatima F, Ahmed MM, Aldawsari MF, Alali AS, Kalam MA, Alshamsan A, Alkholief M, Malik A, Az A, Al-Shdefat R. Abemaciclib-loaded ethylcellulose based nanosponges for sustained cytotoxicity against MCF-7 and MDA-MB-231 human breast cancer cells lines. Saudi Pharm J. 2022;30:726-734.
19. Pathak N, Singh P, Singh PK, Sharma S, Singh RP, Gupta A, Mishra R, Mishra VK, Tripathi M. Biopolymeric nanoparticles based effective delivery of bioactive compounds toward the sustainable development of anticancerous therapeutics. Front Nutr. 2022;9:963413.
20. Yang HB, Song W, Chen LY, Li QF, Shi SL, Kong HY, Chen P. Differential expression and regulation of prohibitin during curcumin-induced apoptosis of immortalized human epidermal HaCaT cells. Int J Mol Med. 2014;33:507-514.
21. Osmani RA, Hani U, Bhosale RR, Kulkarni PK, Shanmuganathan S. Nanosponge carriers- an archetype swing in cancer therapy: a comprehensive review. Curr Drug Targets. 2017;18:108-118.
22. Baburaj R, Veerabhadrappa RS, Das K. Alpha amyrin nano-emulsion formulation from stem bark of *Ficus benghalensis* and its characterization for neuro-behavioral studies. Turk J Pharm Sci. 2024;21:42-51.